Journal of Luminescence 177 (2016) 1–8

Contents lists available at ScienceDirect

Journal of Luminescence

journal homepage: www.elsevier.com/locate/jlumin

Full Length Article

Characterization of the optical gain in doped polymer optical fibres

I. Parola [a], M.A. Illarramendi [a,*], J. Arrue [b], I. Ayesta [c], F. Jiménez [c], J. Zubia [b], A. Tagaya [d], Y. Koike [d]

[a] Department of Applied Physics I, University of the Basque Country UPV/EHU, E.T.S.I. de Bilbao, Alda. Urquijo s/n, E-48013 Bilbao, Spain
[b] Department of Communications Engineering, University of the Basque Country UPV/EHU, E.T.S.I. de Bilbao, Alda. Urquijo s/n, E-48013 Bilbao, Spain
[c] Department of Applied Mathematics, University of the Basque Country UPV/EHU, E.T.S.I. de Bilbao, Alda. Urquijo s/n, E-48013 Bilbao, Spain
[d] Faculty of Science and Technology, Keio University, 3-14-1 Hiyoshi, Kohoku-ku, Yokohama 223-0061, Japan

ARTICLE INFO

Article history:
Received 30 December 2015
Accepted 5 April 2016
Available online 11 April 2016

Keywords:
Light-emitting polymers
Polymer optical fibers
Amplified spontaneous emission
Optical gain
Variable stripe length method
Rhodamine 6G

ABSTRACT

The properties of the amplified spontaneous emission in rhodamine-6G doped graded-index polymer optical fibres of two different dopant concentrations have been analyzed by using the Variable Stripe Length method, both theoretically and experimentally. A theoretical model based on the laser rate equations describes the dependence of the emitted spectrum on the pumped length successfully. The fibre gains and their dependence on the dopant concentration have been analyzed.

1. Introduction

Solid-state organic lasers and amplifiers based on the incorporation of functional materials in an appropriate host, such as a polymer optical fibre (POF), have constituted an attractive research field over the last few years [1,2]. Doped POFs have a number of advantages over their glass counterparts. On the one hand, mechanical strength is higher in polymer materials than in glass, and the fabrication technology is also simpler and cheaper. On the other hand, the much lower manufacturing temperatures of POFs make it possible to embed a variety of functional dopants into the fibre core [3,4], ranging from organic dyes or conjugated polymers, rare earths ions and quantum dots to noble-metal nanoparticles. In addition, the waveguide structure of optical fibres provides several advantages, such as optical confinement in the core area, long interaction distance between the light and the gain medium, symmetric output of the beam profile, good adaptability to fibre-optic communications systems and high ratio between surface area and volume, which allows efficient heat dissipation and minimization of thermal degradation of performance.

The first amplifier based on organic-dye-doped POFs was obtained in 1993 by researchers from Keio University (Japan) who reported a signal gain of 27 dB at 591 nm from a 0.5 metre-long fibre [5]. Since then, the optical gains have been improved in several ways, for example by increasing the dopant concentration in the core material in order to heighten the gain or by employing other dopants in other to amplify a different range of wavelengths. Optical amplifiers based on dye-doped POFs provide a broad spectral gain, which could be used, for example, to amplify all the channels in a wavelength division multiplexing system. In such devices, the gain is due to amplified spontaneous emission (ASE). This phenomenon has been studied both theoretically and experimentally in dye-doped POFs by exciting them either longitudinally or transversely to the fibre symmetry axis [6–11]. ASE presents some of the properties of laser radiation, such as spectral narrowing, existence of a threshold-like energy and directionality, but its output bandwidth is broader than the typical laser radiation. These properties make the doped fibres themselves suitable to be used as broadband fibre sources without laser modes (ASE fibre lasers or mirrorless fibre lasers), with applications in spectroscopy, low coherence interferometry or as sources for fibre gyroscopes [12–14]. A way to investigate the spectral characteristics and irradiance of the light emitted from active fibres consists in analyzing their ASE gain. In spite of the interest of such analyses, there are few reports in which ASE gain in POFs is thoroughly studied [15]. In the case of POFs created in the nanoscale by means of the electrospinning technique, ASE gain properties in both bundles and single fibres have recently been investigated [16–18].

In this work, we present a theoretical and experimental study of the ASE gain following the Variable Stripe Length (VSL) method. This method was first described by Shaklee and Leheny in 1971

* Corresponding author.
E-mail address: ma.illarramendi@ehu.eus (M.A. Illarramendi).

http://dx.doi.org/10.1016/j.jlumin.2016.04.009

[19], and it has proved to be a very useful tool to determine the net gain in active fibres and waveguides. It consists in pumping a stripe of light of adjustable length onto the side of the doped fibre in order to study the dependence of the emitted light irradiance on the length of the stripe. The analyzed fibres are two graded-index (GI) POFs doped with rhodamine 6G (R6G) at different concentrations. Specifically, we have measured and analyzed the spectral peaks, widths and irradiances of the emitted spectra, as functions of the illuminated length. We have also calculated the optical gains at several emission wavelengths. The theoretical model has been carried out by means of the rate equations for the emitted light power and the electronic populations, in terms of time, distance travelled by light along the fibre, light wavelength, and illuminated fibre length. In the analysis, it has been taken into account that the fibres analyzed are the typical GI POFs in which the radial distributions of light power density and dye density are not uniform. The main goal of this work is to show together, for the first time, theoretical and experimental results of the influence of the illuminated length on the emitted spectra from doped POFs.

2. Experimental set-up

The samples analyzed are two GI poly(methyl methacrylate) (PMMA) POFs doped with R6G in the fibre core, the average dopant concentration being 12 ppm in one of the POFs and 16 ppm in the other. In these fibres, the variation of the refractive index is the typical one of a GI POF, as shown in Fig. 1(a), and the dopant concentration is also non-uniform, with greater concentrations at smaller radial distances (see Fig. 1(b)). These fibres were manufactured by some of the authors using the interfacial-gel polymerization technique, in which an unreactive component was employed to obtain the quadratic refractive-index distribution [20]. Specifically, a monomer with a low refractive index (methyl methacrylate) was mixed with an unreactive component with a high refractive index (bromobenzene) to obtain a gradient index in the radial direction, as described in [20]. The mixture also included R6G. The solubility of this dye in methyl methacrylate was enhanced by adding 1.0-wt% of dimethyl sulfoxide. A PMMA tube, whose outer and inner diameters were 10 and 6–7 mm, respectively, was filled with the mixture. This allowed us to have a PMMA cladding. The preform rod was heat-drawn into a fibre. For this purpose, it was moved down into a furnace, set at 180–220 °C, with a constant velocity of about 10 millimetres per minute, while it was also drawn from the bottom with a take-up reel at approximately 5 metres per minute. The POF diameter was controlled by the ratio of these speeds [21]. In our samples, the diameters of the fibre cores are 0.580 mm in the case of the lower concentration and 0.708 mm in the case of the higher one. The total fibre diameter including the cladding is 1 mm in both cases. In both fibres, the refractive index at the fibre symmetry axis is $n_1=1.501$ and it decreases to $n_2=1.492$ in the cladding (see Fig. 1 (a)). For our measurements, these fibres were cut into samples of similar lengths (about 25 cm), whose ends were carefully hand-polished with polishing papers.

Fig. 2 shows the experimental set-up employed to measure the spectra emitted from the fibre using the VSL method. The pump light was the output (532 nm) of a frequency-doubler of a 10 Hz Q-switched Nd:YAG laser (EKSPLA NL301HT). This emits approximately Gaussian pulses whose temporal width at half maximum is about 20 ns. The pulse energy was controlled by inserting calibrated neutral density filters into the beam path. The size and shape of the light beam were controlled by means of two optical lenses (L1 and L2). A cylindrical lens (L3) was used to focus a rectangular light beam onto the fibre side. The illuminated area was 1 mm in height and a variable length z_e in width. This length was adjusted by means of a sliding blade (SL) that was located in the path between the pump laser and the fibre, and which could be moved stepwise by using a motor. In this way, the emission from the fibre was measured for a set of values of z_e in the range between 0 and a certain maximum length $z_{e,max}$ corresponding to the absence of blockage. The distribution of energy of the incident pulse along z_e can be assumed to be uniform, so, as long as the pump energy is not varied as z_e is increased, the impinging light irradiance onto the fibre will remain approximately constant. In all our measurements, the emitted light always propagates through a non-excited length z_{ne} before reaching the detector, due to the size of the connector at the fibre end ($z_{ne}=3.2$ cm). We employed a fibre-optic spectrometer (Ocean Optics USB4000, with an optical resolution of 1.5 nm of full width at half maximum) for the measurement of the emission spectra obtained from one of the fibre ends. When the signal coming from the fibre end was too high, optical filters were inserted into a filter holder (Avantes FH-Inline-1") so as to facilitate light coupling in the spectrometer.

The absorption spectra of the doped fibres were obtained from a Cary 50 UV–VIS spectrophotometer equipped with a fibre-optic coupler accessory. In such measurements, the fibre length was short enough (1 cm) to detect the absorption bands of the dyes embedded in the fibre cores.

3. Background theory

We use the well-known laser rate equations for the generated power and the excited population density [6,7] in order to describe the behaviour of the doped fibre when applying the VSL method. As a first approach, the active material is depicted as a two-level system, which is a reasonable simplification for the organic dyes typically employed in POFs, such as R6G. Our model takes into account that the light power propagates along the fibre in both directions, i.e. towards the detector in the positive z direction and also towards the opposite end of the fibre (see Fig. 2). Let P^+ be

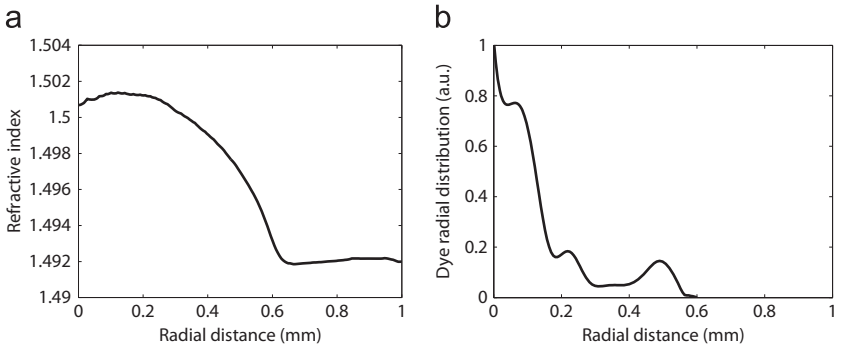

Fig. 1. Refractive index (a) and normalized dye radial distribution (b) in the fibre core as functions of the radial distance.

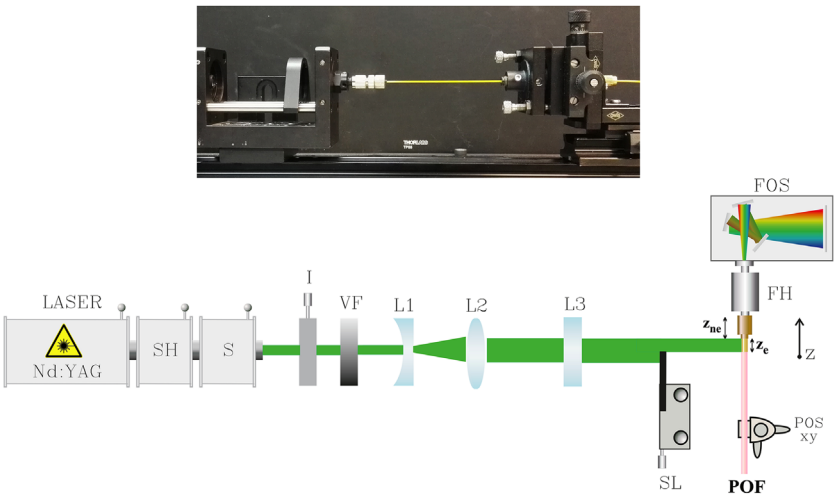

Fig. 2. Experimental set-up for the measurement of the fibre gain using the VSL method. Legend: Nd:YAG: laser; SH: second harmonic generator; S: beam splitter; I: iris; VF: variable filters; L1: divergent lens; L2: convergent lens; L3: cylindrical lens of $f=+15$ cm; SL: sliding blade; POSxy: micro-positioners; FH: filter holder; FOS: fibre-optic spectrometer. Inset: Photograph of the fibre in the experimental set-up.

the light power propagating in the $+z$ direction and P^- the one propagating in the $-z$ direction. Even if P^- itself will not reach the detector, it will excite dopant molecules whose spontaneous and stimulated emissions contribute to increasing the value of P^+ detected from the fibre end closest to the detector. The model also considers that the fibre is graded-index by including an overlapping factor γ in the rate equations in order to describe the stronger interaction between dopant and light in the proximity of the fibre symmetry axis [2]. However, several phenomena that occur in the real fibre are not taken into account in the rate equations, such as the scattering of the transversely pumped light in all directions or the refractions at the interfaces. The evolution of excited population density N_2, P^+ and P^- with t and z for each λ is governed by the following rate equations [7]:

$$\frac{\partial N_2(t,\ z)}{\partial t}=\int_0^{\infty}\frac{P^+(t,z,\lambda)+P^-(t,z,\lambda)}{hf}\gamma\left[\sigma^a(\lambda)\cdot(N-N_2(t,z))-\sigma^e(\lambda)\cdot N_2(t,z)\right]df-\frac{N_2(t,z)}{\tau} \tag{1}$$

$$\frac{\partial P^{\pm}}{\pm\partial z}=\sigma^e(\lambda)\cdot N_2P^{\pm}\gamma-\sigma^a(\lambda)N_1P^{\pm}\gamma-\frac{1}{c/n}\frac{\partial P^{\pm}}{\partial t}+\frac{N_2}{\tau}\left(h\frac{c}{\lambda}\right)\sigma^e_{sp}(\lambda)\beta A_{core} \tag{2}$$

where h is Planck's constant; f is the light frequency; $\sigma^a(\lambda)$ and $\sigma^e(\lambda)$ are the absorption and emission cross sections of the dopant; and τ is the spontaneous lifetime of the dopant in the excited state. The second expression represents two equations, in which the symbol $\pm$ denotes $+$ or $-$, depending on the propagation direction of light; c is the speed of light in vacuum; n is the maximum core refractive index; β is the average value of the fraction of spontaneous emissions that are guided along the GI fibre, as calculated in [2]; $\sigma_{sp}{}^e(\lambda)$ is the spontaneous emission cross section, i.e. the probability distribution of the wavelengths of spontaneously-emitted photons; and A_{core} is the area of the fibre core.

As for the boundary conditions, the pump light impinges transversely onto the fibre, illuminating a length z_e with a temporal Gaussian pulse whose effective width is σ. Its equation is given by:

$$P_p(t)=\frac{E_{p,\ max}(z_e/z_{e,\ max})}{\sigma\sqrt{2\pi}}e^{\frac{-(t-t_{peak})^2}{2\sigma^2}}\quad(\text{for } z\in[0,\ z_e]) \tag{3}$$

where $E_{p,max}$ is the maximum pulse energy impinging on the fibre, i.e. it is the energy E_p for $z_e=z_{e,max}$, and t_{peak} is the instant of maximum lasing power, which is taken to be far enough from 0 for the pulse to have negligible power at $t=0$. Regarding the initial conditions, we assume that there is no light power propagating in the fibre and no excited population at $t=0$. The equations are solved numerically for all considered times t and wavelengths λ along the whole fibre length, which includes various sections: the illuminated length z_e, the non-excited length closest to the detector (z_{ne} in Fig. 2) and even the fibre length on the other side of z_e.

Our model provides the values of N_2 and $P^{\pm}(\lambda)$ for each position z along the fibre and instant t, which allows us to calculate the gain as a function of z and of t. In contrast, there are some simplified stationary models in which N_2 is considered to be either constant or variable along the illuminated length z_e, but this variation only being due to the saturation effects of light [22,23]. These models yield a constant gain in the former case and a variable one in the latter. For the simplest model in which the gain is constant, the dependence of the power on z_e is given by the following analytical expression for any wavelength λ considered:

$$P(z_e,\ \lambda)=\frac{C(\lambda)}{g(\lambda)}\left(e^{g(\lambda)z_e}-1\right) \tag{4}$$

where $g(\lambda)$ is the net gain coefficient and $C(\lambda)$ is a constant related to the spontaneous emission that is given by $C(\lambda)=N_2A_{core}\sigma_{sp}\beta/\tau$. This equation is the most commonly employed to calculate the net gain in active devices such as optical fibres and waveguides.

4. Results and discussion

The absorption coefficients $\alpha(\lambda)$ in each of our R6G-doped fibres are shown in Fig. 3. As could be expected, the sample with the highest concentration yields the highest absorption coefficient in the spectral region considered. Approximately, the maximum of the strongest absorption band of the dye R6G in both fibres occurs in the spectral region between 490 and 550 nm, which corresponds to the transition from the ground singlet state S_0 to the excited singlet state S_1. The flattened shape of this absorption band can be explained from the contributions of dye monomers and aggregates at the employed concentrations, which tend to broaden the band. Similar flat shapes have been reported for this band in R6G-doped PMMA rods [24]. A much weaker absorption band is detected around 350 nm in both fibres, corresponding to the

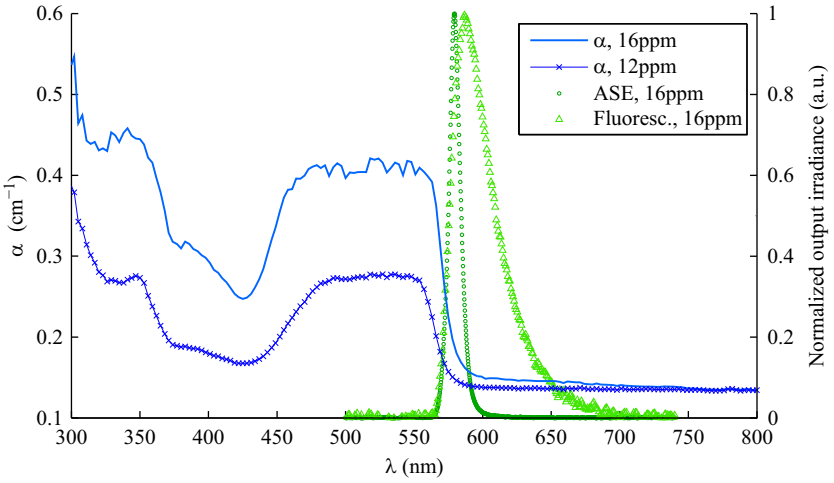

Fig. 3. Solid lines: spectral absorption coefficients (α) corresponding to the 16-ppm POF (thin line) and to the 12-ppm POF ($\times$ -marked line). Triangular marks: normalized fluorescence spectrum obtained with I_p=2.5 mJ/cm^2 and z_e=0.3 cm (E_p=0.075 mJ). Circular marks: normalized ASE spectrum with I_p=2.5 mJ/cm^2 and z_e=2.4 cm (E_p=0.6 mJ).

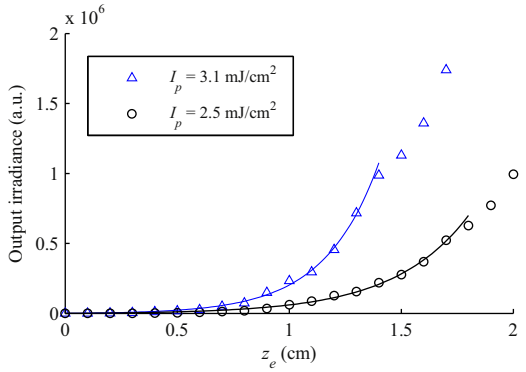

Fig. 4. Output signal measured at λ=570 nm as a function of z_e for two different values of I_p. The measurements have been made with $z_{e,max}$=2 cm. The solid lines are the corresponding least-square fittings to Eq. (4) carried out in the range of values between 0.2 cm and 1.4 or 1.8 cm (depending on I_p).

transition from S_0 to the excited singlet state S_2. Note that this weaker absorption band is superimposed on the ultraviolet tail of the absorption curve of the PMMA host. The values of the absorption curves at wavelengths longer than 700 nm most probably stem from the contribution of light scattering in PPMA and from the experimental method employed. Since the lengths of our measured fibres are very short (about 1 cm), the power mode distributions of the fibres have not yet reached the equilibrium condition, so the attenuations obtained may be higher than those obtained by using long segments as demanded by the standard cut-back method [25]. Fig. 3 also shows the emission spectra experimentally obtained for the 16-ppm fibre for a very short excitation length (z_e=0.3 cm, E_p=0.075 mJ) and for a longer one (z_e=2.4 cm, E_p=0.6 mJ), with the same pump irradiance (I_p) in both cases. The emission curve obtained for the shortest value of z_e, which corresponds to very low pump energy, is the fluorescence curve, whereas the other emission curve is the narrowed emission spectrum with E_p above the ASE threshold energy. In both cases, the emission is due to the transitions from the excited state S_1 to the ground state S_0.

As seen in Fig. 3, the initially broad fluorescence spectrum collapses into a narrow emission band when z_e is increased to a large-enough value at constant pump irradiance. This phenomenon is usually accompanied with an abrupt increase in the output irradiance, as shown in Fig. 4, and it is due to the onset of gain due to ASE. The two curves plotted in Fig. 4 correspond to the 16-ppm fibre and they have been measured at the peak emission wavelength for two pump irradiances. As can be seen, the greater I_p is, the faster the growing of the curves is. Notice that the impinging pump energy is directly proportional to I_p and to z_e. For very small values of either I_p or z_e, the output spectrum would be broad and the output irradiance would be very low. Both the very high output signal and the very narrowed spectrum are indicative of having gone past the ASE threshold, which is usually defined either as the pump energy at which the spectral full width at half maximum (FWHM) decays to half of its maximum value or as the pump energy at which an increase of slope in the growing of the output irradiance is observed [7,14]. To illustrate how the ASE threshold can be estimated, we have plotted both the output irradiances (Fig. 5a) and the spectral widths (Fig. 5b) as functions of the energy absorbed in the fibre (E_{abs}) corresponding to the points of Fig. 4 for the case of I_p=3.1 mJ/cm^2. By applying any of the two definitions just commented, an approximate threshold energy $E_{abs} \approx 0.25$ mJ is obtained for this case. A thorough analysis of ASE thresholds and efficiencies for these types of fibres has been published in [6,7].

An important issue is how much energy is absorbed in the fibre for each pump energy and excitation length. This is shown in Fig. 6, in which the variation of the absorbed energy in the fibre with the incident pump energy has been plotted for all the excitation lengths considered, both in the 16-ppm fibre (Fig. 6(a)) and in the 12-ppm one (Fig. 6(b)). The tendency is for the absorbed energy to be a smaller fraction of the incident one when the concentration is lower, as expected. It can also be noticed that the tendency is also for E_{abs} to increase more slowly with E_p at higher incident pump energies, due to the saturation effects.

4.1. Spectral narrowing

The aforementioned spectral narrowing as z_e is increased has been simulated from Eqs. (1) and (2), using the same optical data (i.e. $\sigma^a(\lambda)$, $\sigma^e(\lambda)$, β, γ, τ, etc.) as in [7] when z_e is varied from 0 to $z_{e,max}$=2 cm in our 16-ppm fibre for various pump irradiances. The shapes of the curves $\sigma^a(\lambda)$, and $\sigma^e(\lambda)$, have been calculated from the absorption and emission spectra measured in our own fibres (see Fig. 3). The absolute values of those curves have been determined using the peak values of the cross sections measured in PMMA bulk as detailed in [26].The theoretical spectral narrowings are shown in Fig. 7(a), and the corresponding experimental results

have been plotted in Fig. 7(b). We can notice that the spectral narrowing with z_e tends to be more rapid when higher pump irradiances are employed. Therefore, the minimum spectral width that will be achieved for a certain z_e (e.g. 2 cm) tends to be smaller for higher values of I_p. This behaviour is the same in both figures. Besides, due to the gain saturation effects, the spectral widths tend to stop narrowing for large-enough values of z_e. Both the theoretical figure and the experimental one show that the spectral width will never be smaller than a certain value (e.g. 10 nm). This tendency is even clearer in the experimental curve corresponding to the maximum I_p, because the greatest gain saturation occurs at the highest pump energies. Similarly, a certain increment in I_p when its initial value is small (e.g. from 3.1 to 5.2 mJ/cm^2) can be approximately as influential as a much larger increment in I_p when its initial value is larger (e.g. from 5.2 to 12.5 mJ/cm^2). This effect is observed both in the theoretical calculations and in the experimental ones. In all cases, the effect of increasing I_p on the spectral width tends to become negligible when z_e is close to 0. This is because the number of excited dopant molecules and the distance travelled by light are not large enough for net gain to occur, so the output from the fibre when z_e is small mainly consists of spontaneous emissions.

The concentration of the dopant also plays an important role in the spectral narrowing, as can be seen in Fig. 8 for our two fibres. For example, Fig. 8(a) shows that the numerically-predicted output spectral width can be considerably broader for a maximum excited length z_e of 2 cm when we employ the 12-ppm fibre instead of the 16-ppm one, which is especially noticeable for the case of the low I_p. For this I_p, it can also be observed that the ASE threshold energy is higher in the case of the 12-ppm fibre. However, if one could increase the impinging pump energy indefinitely, e.g. by increasing I_p or z_e as much as desired, the FWHM of the

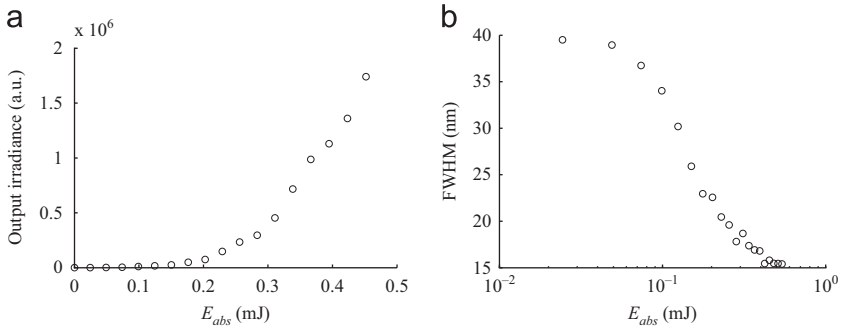

Fig. 5. Experimental output irradiance (a) and FWHM (b) as a function of the absorbed pump energy. The data correspond to the 16-ppm fibre. The measurements have been made with I_p=3.1 mJ/cm^2 by varying z_e.

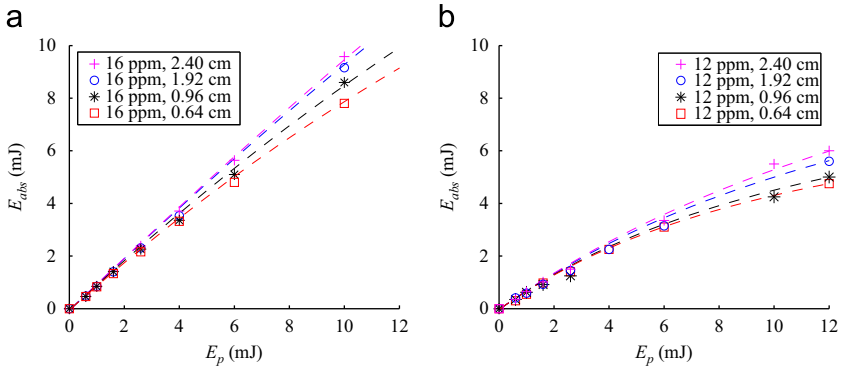

Fig. 6. Experimentally obtained values of the energy absorbed in the fibre as a function of the incident pump energy for four different values of z_e. (a) Case of the 16-ppm fibre and (b) case of the 12-ppm fibre. The dashed lines serve to guide the eye.

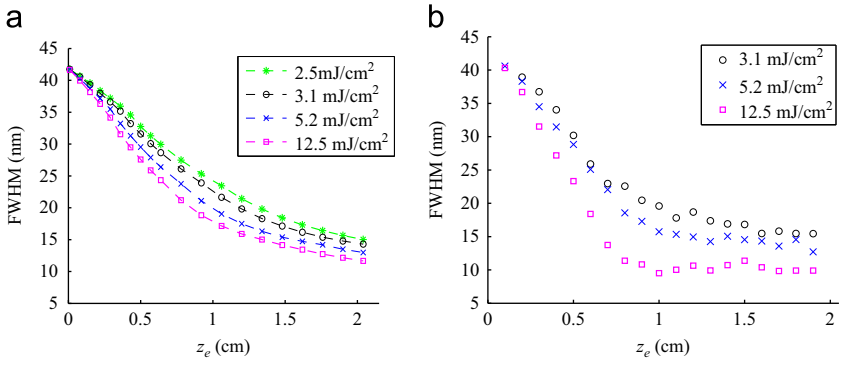

Fig. 7. Theoretical (a) and experimental (b) evolutions of the FWHM of the emission as z_e is increased. Results calculated for the 16-ppm POF and for various pump irradiances I_p.

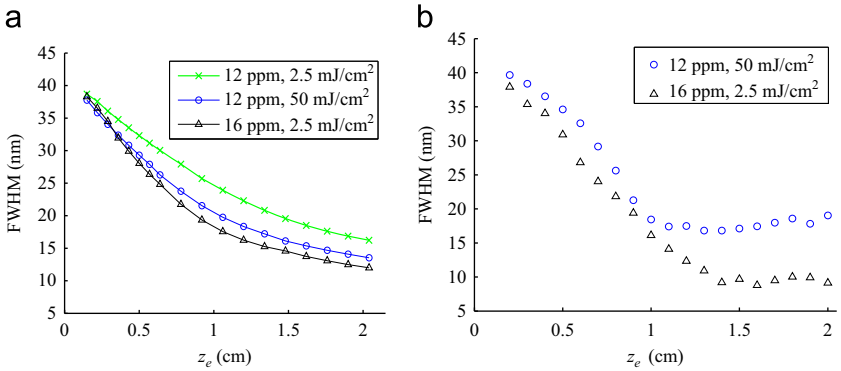

Fig. 8. (a) Theoretical FWHM as a function of z_e for the 12-ppm and 16-ppm POFs excited with two pump irradiances: I_p=2.5 mJ/cm^2 and I_p=50 mJ/cm^2. (b) Experimental FWHM as a function of z_e for the 12-ppm fibre excited with the high I_p and for the 16-ppm fibre excited with the low I_p.

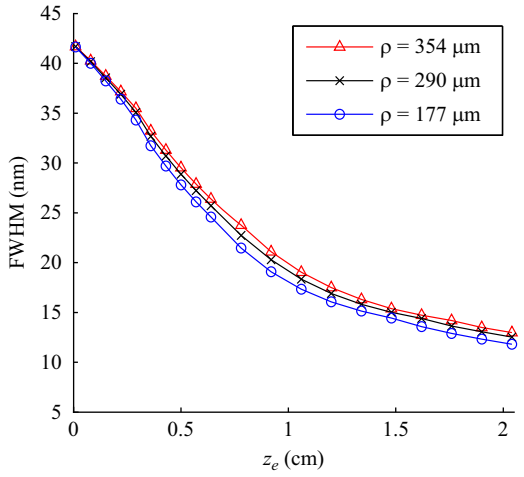

Fig. 9. Theoretical FWHM as a function of z_e for different core radii. The calculations have been made with the data corresponding to the 16-ppm POF with I_p=6 mJ/cm^2.

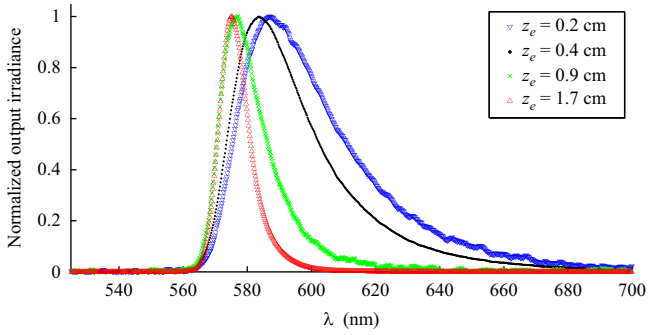

Fig. 10. Output emission spectra obtained from the 16-ppm fibre for various values of z_e with I_p=3.1 mJ/cm^2.

output would never become narrower than a certain value, due to saturation effects (see the tendency in Fig. 8(a) and (b)). Another question that arises is whether there exists a limiting dopant concentration from which a further increase could become irrelevant or even disadvantageous. Indeed, there are motives to expect that, because organic dopants tend to undergo greater aggregation between molecules at very high concentrations, and the molecular interactions could lead to photoluminescence quenching [14]. However, the two concentrations analyzed in this paper are not great enough for this quenching to be noticeable. For such concentrations, I_p has to be much higher in order to compensate for the lower concentration if we are to obtain similar spectral widths, e.g. between 10 and 15 nm, as predicted in Fig. 8 (a). The experimental curves of Fig. 8(b) also show this behaviour, in the sense that the 12-ppm fibre tends to yield a much broader spectrum even when the pump irradiance is higher. It should be noted that the curves of FWHM tend to become rather horizontal for large-enough values of z_e. As has been mentioned, these effects are due to gain saturation, which appears at lower pump energies (i.e. smaller values of z_e) when the concentration is lower.

On the other hand, the larger core radius (ρ) of the 16-ppm POF in comparison with that of the 12-ppm POF might have been a disadvantage to obtain the aforementioned greater spectral narrowing, because the light power density decreases as the core radius increases or, equivalently, as the active volume increases. However, the greater concentration seems to be the dominant factor by far. Indeed, the influence of the core radius has been numerically analyzed keeping constant both the fibre concentration and the pump irradiance, and we have obtained that, although a smaller radius may favour the spectral narrowing, the influence of this effect is relatively small (see Fig. 9).

To finish this section, we would like to mention that the spectral narrowing with z_e is always accompanied by shifts in the emission spectra. Specifically, the output spectra obtained with constant I_p tend to shift towards shorter wavelengths as z_e is increased (see Fig. 10). The evolution of these shifts with z_e takes a shape that is similar to that of the spectral widths. The strong overlap between the absorption curve and the emission spectrum in R6G-doped POFs (see Fig. 3) is responsible for these shifts [27]. More details about the ASE spectral widths and shifts in these types of fibres have been published in [6,7].

4.2. Calculation of the net gain

In Fig. 11(a) we have plotted the calculated energy $E(z)$ of the light at the peak emission wavelength at different positions z along the 16-ppm fibre as we move towards the detector, starting from the edge of the excited length and finishing at the fibre end, and thus including both the points inside the gain volume, from 0 to z_e, and the points outside the gain volume along z_{ne}. Since light is collected from the end at $z=z_e+z_{ne}$, we have only plotted the energy $E(z)$ that propagates in the $+z$ direction (indicated in Fig. 3). Three curves of $E(z)$ have been plotted, each one for different values of $z_{e,max}$ (0.64 cm, 2.4 cm and 3 cm) and of E_p, but maintaining the same pump irradiance in all three cases (I_p=8 mJ/cm^2). When $z_{e,max}$ is 2.4 cm or 3 cm, we can see that $E(z)$ tends to increase exponentially in the illuminated length, with the exception of the region of the small values of z and of the largest values (very close to $z_{e,max}$). As is well known, the density of excited molecules (N_2) is smaller at both sides of the active volume than towards its centre. The amount of stimulated emissions is not only proportional to $N_2(z)$ but also to $E(z)$, which is

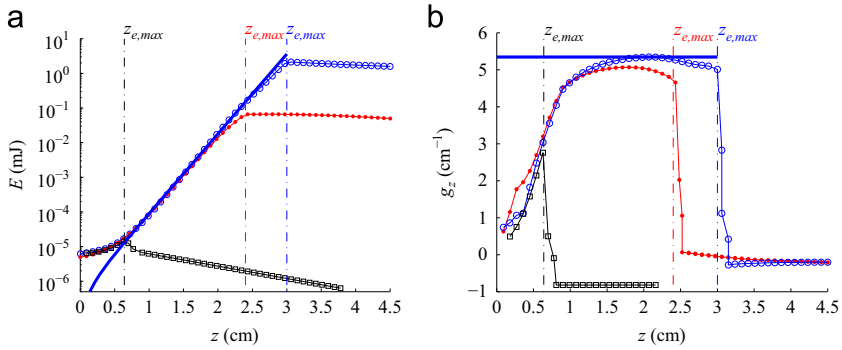

Fig. 11. (a) Evolution of the local energy with z for three different values of $z_{e,max}$ (squares: 0.64 cm, dots: 2.4 cm, empty circles: 3 cm), maintaining the pump irradiance constant (I_p=8 mJ/cm^2), (b) evolution of the local net gain with z obtained as the slopes in (a), with the same notation. Solid line in (a): theoretical curve obtained from Eq. (4). Horizontal line in (b): theoretical constant gain corresponding to Eq. (4).

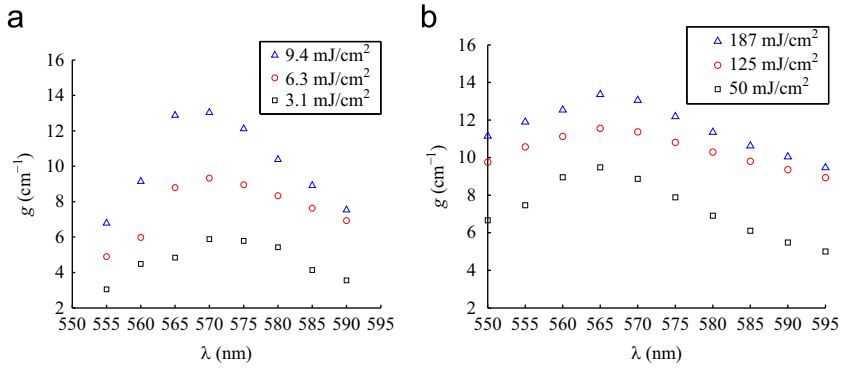

Fig. 12. (a) Spectral gains for the 16-ppm POF pumped with three irradiances; (b) spectral gains for 12-ppm POF pumped with other three irradiances.

negligible at z=0 if we only consider the photons propagating in the $+z$ direction. As a consequence, the probability of stimulated emissions in the $+z$ direction also decreases in the proximity of z=0, which explains the slower increase in $E(z)$ for the smallest values of z [13]. This fact also explains the different behaviour of the curve for $z_{e,max}$=0.64 cm in the figure, which increases rather slowly in its whole interval of values of z_e due to the fact that both the distances travelled by photons and the available number of dopant molecules are too small for stimulated emission to dominate over spontaneous ones. In all cases, the curve of $E(z)$ tends again to become a straight line outside the gain volume, but of negative slope, which corresponds to a negative net gain.

Fig. 11(b) shows the evolution of the net gain at each z, or local net gain $g_z=d(\log E)/dz$, obtained as the slopes in Fig. 11(a). As can be seen when $z_{e,max}$ is 2.4 cm or 3 cm, there is a zone of rather constant positive gain from a certain minimum value of z to nearly $z_{e,max}$, coinciding with the straight segment of positive slope in Fig. 11(a). As z approaches $z_{e,max}$, the onset of gain saturation can be observed, since the values of $g_z(z)$ begin to decrease. For $z > z_{e,max}$, there is another zone of rather constant negative gain, which coincides with the straight segment of negative slope in Fig. 11(a). There is a very rapid transition zone in the change from positive to negative gains.

In our measurements, we collect the light that has travelled all the fibre length z_e+z_{ne}, thus crossing zones of positive and of negative local gain $g_z(z)$. If we consider that the absolute values of $g_z(z)$ are much smaller in z_{ne} than in z_e, we can see that the contribution of the non-illuminated length to the output energy is relatively negligible. The negative net gain in such length (z_{ne}) is due to the fibre losses and it tends to be equal, in absolute value, to the absorption coefficient α of the fibre. By using the side-illuminated fluorescence technique [25,28], we have measured that the value of α in the 12-ppm POF is 0.25 cm^{-1} at 578 nm, which is in agreement with the values shown in Fig. 3 and confirms that the losses in z_{ne} are much smaller than the gain in z_e. Therefore, the fibre output could be estimated from the behaviour of light only in the illuminated segment. When $z_{e,max}$ is large, $g_z(z)$ becomes constant along a large enough length to be able to assume a constant g inside the illuminated segment, as is done in Eq. (4). As an example, the theoretical evolution of the local energy $E(z)$ obtained from Eq. (4) and its corresponding constant gain g have been included in Fig. 11 for the case of $z_{e,max}$=3 cm at the peak emission wavelength. The constant $C(\lambda)$ of Eq. (4) has been arbitrarily chosen in order to be able to compare the shape of this approximate $E(z)$ with the one obtained from the rate equations (see the solid line and the circle-marked line in Fig. 11(a)). As can be seen, the slopes of both lines are the same, with the exception of the largest and of the smallest values of z, corresponding to the onset of the gain saturation and to the initial transitory growth of the generated light energy, respectively. For the smallest values of z, the local gain is variable, so it is convenient to employ values of z_e that are not very close to 0 in order to obtain the constant gain g from Eq. (4). Taking these considerations into account, we have calculated the spectral gains of the two fibres from the fittings of the experimental output irradiances to Eq. (4). Specifically, these fittings have been calculated avoiding the irradiances measured both at the shortest and at the largest values of z_e. An example of this procedure can be seen in Fig. 4, in which the fittings of the output irradiances of the 16-ppm fibre have been included. As can be seen, the output irradiances increase as predicted by Eq. (4), with the exception of the largest values of z_e, in which we can notice that the gain is saturated.

Fig. 12 shows the spectral gains of our two fibres calculated from the fittings of the evolutions of the output irradiances for each of the desired emission wavelengths as z_e is increased, in the way that has been explained. The results for the 16-ppm POF are

shown in Fig. 12(a) and those for the 12-ppm POF are plotted in Fig. 12(b). As can be seen at all wavelengths for both fibres, greater gains are achieved with greater excitation irradiances, although, in all cases, the maximum gain takes place at a wavelength λ that lies in the range between 565 and 570 nm. In spite of the much greater pump irradiances employed with the 12-ppm fibre, the gains obtained with both fibres are similar, confirming the strong influence of the dopant concentration on the ASE processes that take place in these doped fibres. The values of the gains obtained in our fibres (Fig. 12) are comparable to those reported in electrospun R6G-doped PMMA nanofibres [18].

5. Conclusions

We have reported the Amplified-Spontaneous-Emission properties in rhodamine-6G doped graded-index polymer optical fibres of two different dopant concentrations by using the Variable Stripe Length method. We have shown that our theoretical model based on the laser rate equations can serve to explain the narrowing of the emission spectra measured as the excited length is increased with constant pump irradiance. It can also serve to explain the influence of the pump irradiance and of the dopant concentration on the output spectrum. For the analyzed dopant concentrations (12 ppm and 16 ppm), we have seen that the concentration plays an important role in the emission spectrum. In the case of the lower concentration, the ASE threshold is higher, and the spectral width achieved is broader. Moreover, the pump irradiance has to be much higher in the fibre with lowest concentration in order for the output spectral widths to be similar to those obtained with the highest concentration, e.g. between 10 and 15 nm. Finally, we have shown that a constant gain can be assumed to describe the evolution of the output irradiances with the excited length z_e as long as the smallest and the largest values of z_e are omitted, which correspond to the transitory growth of the ASE and to the gain saturation region, respectively. By carefully fitting the output irradiances, we have calculated the ASE gains at several emission wavelengths. The gains obtained show that a maximum value of nearly 14 cm^{-1} can be achieved with a pump irradiance of 9.4 mJ/cm^2 in the case of the 16-ppm POF, whereas a much higher pump irradiance (of about 187 mJ/cm^2) is needed to achieve the same maximum gain in the case of the 12-ppm POF, thus confirming the importance of the dopant concentration on the achievable fibre gain.

Acknowledgements

This work has been funded in part by the Fondo Europeo de Desarrollo Regional (FEDER) by the Ministerio de Economía y Competitividad under project TEC2015-638263-C03-1-R; by the Gobierno Vasco/Eusko Jaurlaritza under projects IT933-16 and ELKARTEK; by the University of the Basque Country UPV/EHU under programmes UFI11/16 and Euskampus; and by the Japan Society for the Promotion of Science through the Funding Program for World-Leading Innovative R&D on Science and Technology (FIRST Program), initiated by the Council for Science and Technology. The work carried out by I. Parola has been funded by a research grant given by the Departamento de Educación, Política Lingüística y Cultura del Gobierno Vasco/Eusko Jaurlaritza for her PhD thesis.

References

[1] J. Clark, G. Lanzani, Nat. Photonics 4 (7) (2010) 438.
[2] J. Arrue, F. Jiménez, I. Ayesta, M. Asuncion Illarramendi, J. Zubia, Polymers 3 (3) (2011) 1162.
[3] H. Liang, Z. Zheng, Z. Li, J. Xu, B. Chen, H. Zhao, et al., J. Appl. Polym. Sci. 93 (2) (2004) 681.
[4] H. Liang, Z. Zheng, Z. Li, J. Xu, B. Chen, H. Zhao, et al., Opt. Quant. Electron. 36 (15) (2004) 1313.
[5] A. Tagaya, Y. Koike, T. Kinoshita, E. Nihei, T. Yamamoto, K. Sasaki, Appl. Phys. Lett. 63 (7) (1993) 883.
[6] M.A. Illarramendi, J. Arrue, I. Ayesta, F. Jiménez, J. Zubia, I. Bikandi, A. Tagaya, Y. Koike, Opt. Express 21 (20) (2013) 24254.
[7] J. Arrue, M.A. Illarramendi, I. Ayesta, F. Jiménez, J. Zubia, A. Tagaya, Y. Koike, Photonics J. IEEE 7 (2) (2015) 1.
[8] K. Kuriki, T. Kobayashi, N. Imai, T. Tamura, S. Nishihara, Y. Nishizawa, et al., Appl. Phys. Lett. 77 (3) (2000) 331.
[9] L. Zeng-Chang, L. Hao, Z. Zhi-Qiang, Z. Qi-Jin, M. Hai, Chin. Phys. Lett. 22 (3) (2005) 618.
[10] M. Sheeba, K.J. Thomas, M. Rajesh, V.P.N. Nampoori, C.P.G. Vallabhan, P. Radhakrishnan, Appl. Opt. 46 (33) (2007) 8089.
[11] G.V. Maier, T.N. Kopylova, V.A. Svetlichnyi, V.M. Podgaetskii, S.M. Dolotov, O. V. Ponomareva, A.E. Monich, E.A. Monich, Quantum Electron. 37 (1) (2007) 53.
[12] B. Redding, P. Ahmadi, V. Mokan, M. Seifert, M.A. Choma, H. Cao, Opt. Lett. 40 (2015) 4607.
[13] M.J.F. Digonnet, Rare Earth Doped Fiber Lasers and Amplifiers, Marcel Dekker, Inc, New York, 1993.
[14] E.M. Calzado, P.G. Boj, M.A. Díaz-García, Int. J. Mol. Sci. 11 (2010) 2546.
[15] T. Kobayashi, W.J. Blau, H. Tillmann, H.-H. Hörhold, Opt. Lett. 26 (24) (2001) 1952.
[16] G. Morello, M. Moffa, S. Girardo, A. Camposeo, D. Pisignano, Adv. Funct. Mater. 24 (2014) 5225.
[17] G. Morello, A. Camposeo, M. Moffa, D. Pisignano, Appl. Mater. Interfaces 7 (2015) 5213.
[18] L. Persano, A. Camposeo, P. Del Carro, V. Fasano, M. Moffa, R. Manco, S. D'Agostino, D. Pisignano, Adv. Mater. 26 (2014) 6542.
[19] K.L. Shaklee, R.F. Leheny, Appl. Phys. Lett. 18 (1971) 475.
[20] T. Ishigure, E. Nihei, Y. Koike, Appl. Opt. 33 (19) (1994) 4261.
[21] A. Tagaya, S. Teramoto, E. Nihei, K. Sasaki, Y. Koike, Appl. Opt. 36 (3) (1997) 572.
[22] L. Dal Negro, P. Bettotti, M. Cazzanelli, D. Pacifici, L. Pavesi, Opt. Commun. 229 (2004) 337.
[23] A. Costela, O. García, L. Cerdán, I. García-Moreno, R. Sastre, Opt. Express 16 (10) (2008) 7023.
[24] G. Somasundaram, A. Ramalingam, J. Photochem. Photobiol. A: Chem. 125 (1–3) (1999) 93.
[25] M.A. Illarramendi, J. Zubia, L. Bazzana, G. Durana, G. Aldabaldetreku, J. R. Sarasua, J. Light. Technol. 27 (15) (2009) 3220.
[26] A. Tagaya, T. Kobayashi, S. Nakatsuka, E. Nihei, K. Sasaki, Y. Koike, Jpn. J. Appl. Phys. 36 (1997) 2705.
[27] J. Arrue, F. Jiménez, M.A. Illarramendi, J. Zubia, I. Ayesta, I. Bikandi, A. Berganza, IEEE Photonics J. 2 (3) (2010) 521.
[28] M.G. Kuzyk, Polymer Fiber Optics: Materials, Physics, and Applications, CRC Press, Boca Raton, Fla, 2007.